optica

Chip-based Brillouin processing for carrier recovery in self-coherent optical communications

Elias Giacoumidis,[1,2,5,*,†] Amol Choudhary,[1,2,6,†] Eric Magi,[1,2] David Marpaung,[1,2] Khu Vu,[3] Pan Ma,[3] Duk-Yong Choi,[3] Steve Madden,[3] Bill Corcoran,[4] Mark Pelusi,[1,2] and Benjamin J. Eggleton[1,2,7]

[1]Institute of Photonics and Optical Science (IPOS), School of Physics, University of Sydney, Sydney, NSW, Australia
[2]The University of Sydney Nano Institute, University of Sydney, Sydney, NSW, Australia
[3]Laser Physics Centre, Australian National University, Canberra, ACT, Australia
[4]Department of Electrical and Computer Systems Engineering, Monash University, Clayton, 3800 VIC, Australia
[5]Currently at Dublin City University, Radio and Optical Laboratory, Glasnevin 9, Dublin, Ireland (elias.giacoumidis@dcu.ie)
[6]e-mail: amol.choudhary@sydney.edu.au
[7]e-mail: egg@physics.usyd.edu.au
*Corresponding author: e.giacoumidis@sydney.edu.au

Modern fiber-optic coherent communications employ advanced, spectrally efficient modulation formats that require sophisticated narrow-linewidth local oscillators (LOs) and complex digital signal processing (DSP). Self-coherent optical orthogonal frequency-division multiplexing (self-CO-OFDM) is a modern technology that retrieves the frequency and phase information from the extracted carrier without employing a LO or additional DSP. However, a wide carrier guard is typically required to easily filter out the optical carrier at the receiver, thus discarding many OFDM middle subcarriers that limit the system data rate. Here, we establish an optical technique for carrier recovery, harnessing large-gain stimulated Brillouin scattering (SBS) on a photonic chip for up to 116.82 Gbit · s^{-1} self-CO-OFDM signals, without requiring a separate LO. The narrow SBS linewidth allows for a record-breaking small carrier guard band of ~265 MHz in self-CO-OFDM, resulting in higher capacity than benchmark self-coherent multi-carrier schemes. Chip-based SBS-self-coherent technology reveals comparable performance to state-of-the-art coherent optical receivers while relaxing the requirements of the DSP. In contrast to on-fiber SBS processing, our solution provides phase and polarization stability. Our demonstration develops a low-noise and frequency-tracking filter that synchronously regenerates a low-power narrowband optical tone, which could relax the requirements on very-high-order modulation signaling for future communication networks. The proposed hybrid carrier filtering-and-regeneration technique could be useful in long-baseline interferometry for precision optical timing or reconstructing a reference tone for quantum-state measurements.   © 2018 Optical Society of America under the terms of the OSA Open Access Publishing Agreement

OCIS codes: (060.2330) Fiber optics communications; (060.1660) Coherent communications; (190.0190) Nonlinear optics; (290.5900) Scattering, stimulated Brillouin.

https://doi.org/10.1364/OPTICA.5.001191

1. INTRODUCTION

Modern fiber-optic coherent communications have triggered advanced modulation formats of a higher order than four states, such as 16–128 quadrature amplitude modulation (QAM), requiring sophisticated narrower linewidth (<100 kHz) local oscillators (LOs) compared to common distributed feedback lasers (>1 MHz) [1]. On the other hand, a significant frequency mismatch between the transmitter laser (carrier) and the receiver LO laser occurs in coherent optical transmission systems, which highly impacts the phase-coherence-producing phase noise. More specifically, due to the frequency mismatch of the transmitter laser and the LO, a carrier frequency offset (usually time varying) occurs, and since the transmitter and LO lasers are not phase locked,

this necessitates a carrier phase recovery stage at the receiver. To cancel this frequency mismatch, an extra digital signal processing (DSP) functional block is traditionally employed, which increases the DSP computational load and potentially both electronic processing power [2–4] and latency [5]. This is perceived to be critical for future-proof real-time machine-to-machine communications such as remote medicine, financial trading [5], cloud computing, and the internet of things (IoT).

Whereas previous studies [2–4] tackle the Kerr-induced fiber nonlinearity, which is critical for long-haul coherent optical communications, presently there is no solution to relax the stringent requirements of DSP units and advanced modulation formats in cost-and-energy-sensitive short-reach communications such as

warehouse-scale data centers [6] and access and metropolitan networks [7] (including 5G [8]), which have become coherent-centric to support capacities [9–11] >100 Gbit · s^{-1}. Alternative approaches for practical short-reach coherent communications systems have been demonstrated: for instance, Kramer–Kronig systems [12,13] reduce the receiver optical complexity by utilizing a single photodiode; however, advanced DSP is still required.

Self-homodyne coherent technology [14–23], where the LO laser is transmitted together with the signal, relaxes the requirements for DSP since it eliminates the need for frequency-offset compensation between the transmitter laser and the LO. Yet, for single-carrier modulation, this technology sacrifices one of the two orthogonal polarizations of the fiber to fit an optical carrier that halves transmission capacity. For multi-carrier schemes such as self-coherent optical orthogonal frequency-division multiplexing (self-CO-OFDM) [15,16,20,21,23], it typically requires a large carrier guard band (i.e., frequency gap that discards many OFDM middle subcarriers) for filtering out the carrier that significantly limits signal capacity. Recent carrier recovery solutions employing injection-locked lasers [15,16] and Fabry–Perot filters [21] have been reported, but they lack the spectral resolution required for high spectral efficiency or require high-precision carrier-tracking analog devices at the receiver.

In this paper, we propose to harness large-gain stimulated Brillouin scattering (SBS) [24–26] on a compact photonic chip for ultrahigh-resolution selective filtering for carrier recovery in high-capacity self-coherent optical signals without requiring a separate LO. SBS is processed on a chalcogenide chip to enable sufficiently high gain, thus providing successful extraction and regeneration of the carrier. The ultrahigh-resolution SBS selective filtering of the received carrier increases signal capacity by reducing the carrier guard band between the carrier and the signal band. We report that on-chip SBS demonstrates a high-performance practical ("black-box") "self-tracking" narrowband hybrid amplifier and filter without requiring analog loops. Our demonstration merges for the first time to our knowledge the attractive features of chip-based SBS [24,25] and self-coherent technology.

Previously reported fiber-based SBS-self-coherent systems [27,28] have been limited to single-quadrature modulated formats to avoid excessive phase noise from the interaction of SBS with the processed fiber (typically of long length) that results in polarization drifts, large propagation delays, and increased susceptibility to environmental fluctuations. In comparison, our chip-based approach is free from excessive carrier drifting, providing phase and polarization stability associated with thermal and polarization drifts over the propagation length of the Brillouin gain medium, thus eliminating the need for high-precision carrier-tracking analog devices at the receiver. Due to the narrow linewidth of SBS and the "self-referencing" nature of the proposed technique, a record-breaking narrow carrier guard band of ~265 MHz for a data rate of 116.82 Gbit · s^{-1} is achieved for self-coherent optical signals. Our approach reveals comparable performance to state-of-the-art coherent optical receivers without requiring additional digital techniques.

2. PROOF OF CONCEPT AND COMPARISON WITH BENCHMARK TECHNOLOGIES

The principle of the compact photonic chip scheme for carrier recovery in high-capacity self-coherent optical signals is summarized in Fig. 1. For modulation, we used OFDM [29], which is
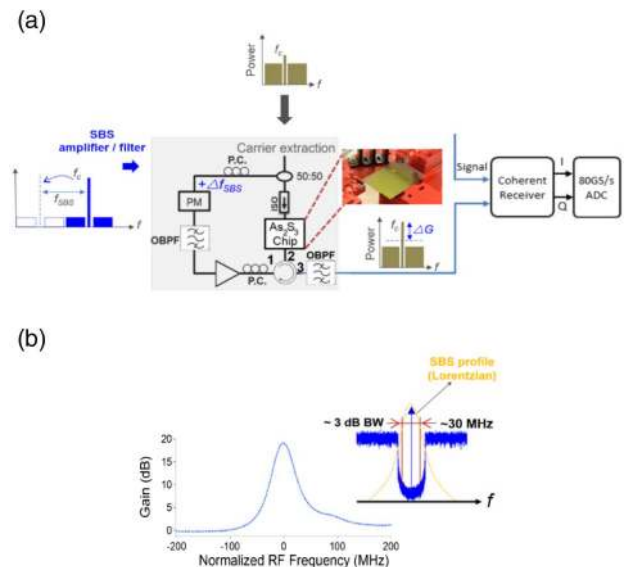
Fig. 1. (a) Receiver SBS-based self-CO-OFDM. (b) Filter gain profile (Lorentzian) and illustration of the filtering process on an OFDM signal spectrum with carrier guard band of ~256 MHz. P.C., polarization controller; (O)BPF, (optical) band-pass filter; ISO, isolator; ADC, analog-to-digital converter; OM, optical modulator; PM, phase modulator; As$_2$S$_3$, chalcogenide.

constituted of megahertz (MHz)-bandwidth subcarriers M_s. To this end, we established an ad hoc SBS-based self-CO-OFDM system as a test case for carrier recovery without requiring DSP carrier recovery. On-chip SBS-self-CO-OFDM harnesses the unique capability of SBS to retrieve frequency, amplitude, and phase information from the extracted carrier without employing a separate LO. The narrow linewidth of SBS and the self-referencing nature of the proposed technique allows for a narrow carrier guard band of ~265 MHz (without considering the bandwidth allocated to the DC carrier), which is set in the middle of the OFDM signal to easily filter out the received carrier. In contrast to benchmark self-CO-OFDM schemes [14–21], our chip-based approach offers a compact stable integrated solution and enhanced signal capacity by reducing the frequency carrier guard band. The SBS filter is free from analog carrier-locking laser devices and electronics [15,16,21] due to the self-tracking nature of the SBS filter formed by using a frequency-shifted copy of the received signal as the pump and has narrowband function (3 dB bandwidth of tens of MHz), which is much tighter than traditional solutions employing injection-locked lasers [15,16] and Fabry–Perot filters [21]. For our experiments, the self-CO-OFDM system was set at a nominal data rate, S_k, of 116.82 Gbit · s^{-1} for 16-QAM and 54.95 Gbit · s^{-1} for quaternary phase-shift keying (QPSK) using 127 generated subcarriers, M_s. Modulation was performed using an IQ-Mach–Zehnder modulator (IQ-MZM) for amplitude (I) and phase (Q) data subcarriers. It should be noted that using Alamouti coding of the signal [30] polarization independency is feasible without a polarizing element in place. While Alamouti coding causes 50% redundancy due to the replication of the transmitted symbols and requires a polarization modulator in the transmitter, it does not require any additional DSP complexity, higher bandwidth, or resolution of the digital-to-analog converters/analog-to-digital

converters (DACs/ADCs). Furthermore, it enables removal of the polarization beam splitter(s)/rotator(s), the 90° optical hybrid, and two of the balanced photodetectors. The polarization-independent single-polarization coherent receiver enabled by Alamouti coding retains many of the advantages of coherent detection, including high power/bandwidth efficiency, linear optical field detection, and robustness to fiber impairments. Another option could be through aligning the carrier with the signal in a single polarization, or speculatively by combining the current scheme with polarization-diverse or independent-injection locking [16].

The OFDM signal was transmitted through a 40 km standard single-mode fiber (SSMF) link, and afterwards, a 50:50 coupler was used at the receiver to separate the OFDM signal path from carrier extraction as depicted in Fig. 1(a). In the carrier extraction path, the SBS selects and amplifies the optical carrier, operating as a narrow-width optical band-pass self-tracking filter (OBPF) that follows a Lorentzian spectral profile as depicted in Fig. 1(b), with a gain measured up to 20 dB for a chalcogenide chip alone using the pump-probe technique described in Ref. [24]. (Note that in the carrier-recovery experiment, a lower gain was achieved. This is because the "signal" power around the pump does not contribute to the SBS amplification). The self-tracking nature of the filter is realized by splitting the signal and using the frequency-shifted version of the signal as the SBS pump. So even if the laser drifts, the SBS pump will drift in the same manner, thus always providing SBS gain on the signal. At the photodetector, the beat between the LO and the signal will not drift in the radio-frequency (RF) domain, thus nullifying the need for frequency-offset compensation.

The SBS gain bandwidth was measured to be only ~30 MHz. In the SBS process, another OBPF of 5 GHz bandwidth selected only the upper sideband, which was amplified and counter-propagated with the other half of the received signal in the photonic chip. The Brillouin amplified carrier was extracted through port 3 of the circulator and the output of the SBS pump was sent to an external OBPF of ~5 GHz bandwidth to primarily remove

the back-reflected pump; it also aids in the increase of the optical carrier-to-signal ratio (OCSR) of the transmitted signal as shown in Fig. 3. This filter can be removed through optimized waveguide fabrication to minimize back-reflections. Finally, the recovered carrier was sent to the LO input of the coherent homodyne receiver, which was connected to an oscilloscope, and the received data were processed offline using Matlab. For our experiments, the Brillouin amplification was performed in a 24.0 cm long chalcogenide (As_2S_3) chip. In the first experiment, the proposed self-CO-OFDM system was compared to a state-of-the-art CO-OFDM, which employs DSP-based phase-noise and frequency-offset compensation. In the second experiment, chip-based SBS was compared to a self-CO-OFDM system with SBS being realized in a 4.46 km long SSMF. For the chip-based approach, SBS gain is measured when the chip is inserted into the signal path and is therefore the ON-OFF gain, measured to be 14 dB. The propagation loss is about 0.2 dB/cm. Characterization for similar chips has been provided in Ref. [31]. The total and individual OFDM M_s subcarriers' bit error rate (BER) by error counting, Q-factor ($= 20 \log_{10}[\sqrt{2}\mathrm{erfc}^{-1}(2\mathrm{BER})]$), and SBS gain were the crucial parameters under investigation. The received signal was also noise-loaded using an amplified spontaneous emission source to measure the Q-factor as a function of the optical signal-to-noise ratio (OSNR).

A qualitative representation and comparison between the developed SBS carrier recovery chip for self-coherent detection, a fiber-based SBS processor, and a state-of-the-art carrier-suppressed coherent system with OFDM is illustrated in Fig. 2. In this block diagram, we show that the proposed chip-based solution can essentially provide less electronic processing compared to the other two approaches. This occurs because, first, chip-based SBS can extract and regenerate the optical carrier from the coherent signal without employing frequency alignment circuitry at the receiver. Second, it only requires electronic dispersion compensation (EDC) and channel estimation at the receiver, eliminating the need for additional DSP for both frequency-offset correction and phase-noise compensation.
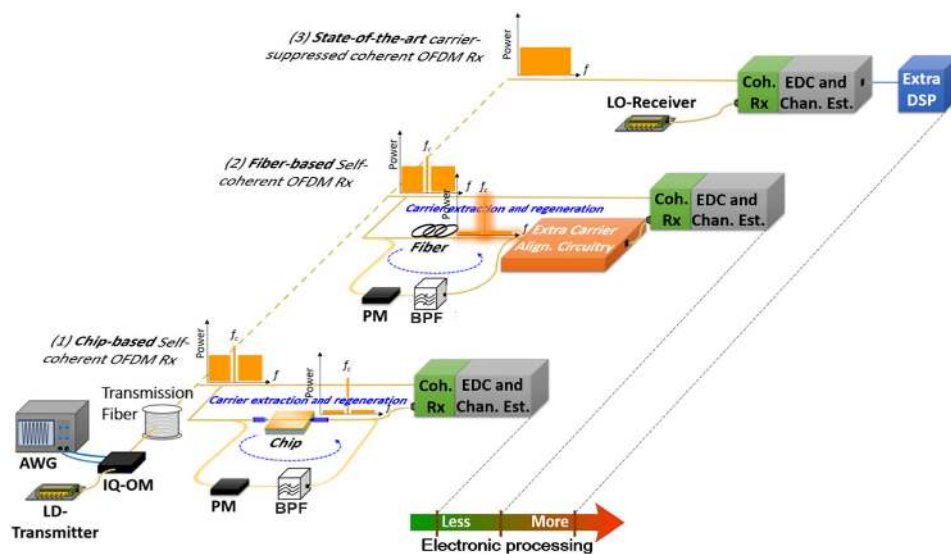
Fig. 2. Qualitative comparison of the developed (1) chip-based self-CO-OFDM system with (2) SBS processed on a fiber, and (3) a state-of-the-art carrier-suppressed CO-OFDM. AWG, arbitrary waveform generator; LD, laser diode; OM, optical modulator; PM, phase modulator; EDC, electronic dispersion compensation; LO, local oscillator; DSP, digital signal processing.

3. METHODS

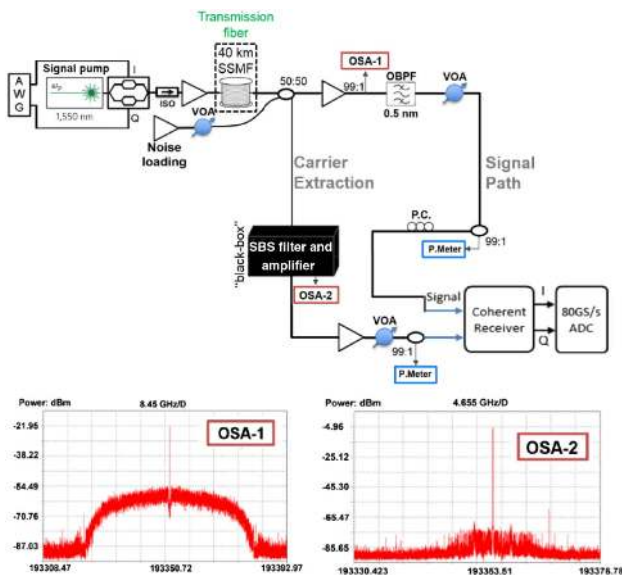Below we provide more details about the experimental and simulation setups.

A. Experimental Setup

In Fig. 3, the self-CO-OFDM experiment is depicted including the SBS-based black box. From the inset optical spectrum analyzer-1 (OSA-1) of Fig. 3, the OCSR was measured around −3 dB (at 5 MHz spectral resolution). It should be indicated that the optical signal power in our OSNR measurement is the combined signal and carrier power; hence, the ratio of the actual OSNR to the measured OSNR is 1+OCSR (using linear ratios). In Fig. 4, the experimental setup of the conventional 16-QAM CO-OFDM is depicted in which a LO is implemented at the receiver. The OCSR for the CO-OFDM was set at −22 dB (below and above which the system performance is degraded). In more detail, the baseband waveform samples were calculated offline based on a pseudo-random binary sequence of 2^{19-1}. In the transmitter, an arbitrary waveform generator was used at a sampling rate, r_s, (frequency bandwidth) of 34 GHz to generate a continuous self-CO-OFDM or conventional CO-OFDM baseband signal. The frequency spacing from center-to-center k-subcarrier was estimated at ∼133 MHz. For the generation of the OFDM signal, a 256 inverse fast Fourier transform (IFFT) size was implemented from which 128 subcarriers (1000 symbols per subcarrier)

Fig. 3. SBS-based self-CO-OFDM experimental setup block diagram. Insets: optical spectrums from transmitter side (OSA-1) and after carrier selection (OSA-2). OSA, optical spectrum analyzer; VOA, variable optical attenuator; P. Meter, power meter.

Fig. 4. Experimental conventional CO-OFDM block diagram that includes the transmission link and noise loading.

were employed as data and the rest were set to zero (highest 128 frequencies) in order to separate the OFDM baseband signal from the aliasing products generated at the output of the DACs. The modulation format was either QPSK or 16-QAM (with the total number of binary bits, n_k, to be 2 and 4, respectively), and only 1 subcarrier around the direct current (DC) component was padded with zero (carrier guard band) to enable a spectral guard band within OFDM subcarriers in self-CO-OFDM and allow the insertion of an optical carrier (i.e., [128−1] M_s subcarriers). A cyclic prefix overhead of 10% was inserted to increase inter-symbol interference tolerance. Three percent of the signal band was sacrificed for channel estimation (pilot-aided) for both QPSK and 16-QAM, and no carrier frequency offset was required. Therefore, the nominal data rates, S_k, resulted in 54.949 Gbit · s^{-1} (QPSK) and 116.82 Gbit · s^{-1} (16-QAM) for self-CO-OFDM.

In the optical domain, a tunable external cavity laser with a linewidth of ∼100 kHz (this value is lower than the SBS gain bandwidth, allowing stable operation condition) was used at the transmitter to generate a continuous wave signal at ∼1550 nm (signal pump, ωp) that was subsequently modulated with the self-CO-OFDM signal by an IQ-MZM, biased such that the carrier was not totally suppressed. We should note that since the modulator can operate at a constant temperature using a thermoelectric cooler, then there is no need for feedback to a bias controller, as bias remains stable. The launched optical power for both on-chip and SMF-based self-CO-OFDM systems and CO-OFDM was set at 0 dBm. After transmission through 40 km of SSMF link, a noise source was placed using an erbium-doped fiber amplifier (EDFA) to adjust the OSNR at a desired value. At the receiver, a 50:50 coupler was used to separate the OFDM signal path from the carrier extraction path. In the carrier extraction path, the SBS pump extracts and amplifies the carrier where we counter-propagated the frequency-shifted signal in the SBS medium. Another 50:50 coupler was used to split the light in the carrier extraction path with half of the light being modulated by a phase modulator (PM) to shift the incoming light by the Brillouin–Stokes shift. In fiber, the Brillouin shift is 10.86 GHz [26], while for the on-chip chalcogenide waveguide, the shift is 7.7 GHz [24]. The output of the SBS pump was sent to a combined EDFA with a variable optical attenuator (VOA) as a safety measure to protect the coherent receiver from any fluctuations in carrier power (∼0.5–0.7 dB) due to SBS gain variations from polarization or other environmental effects. This was subsequently incident on a 90° optical hybrid and emulated as a LO. The polarization of the extracted optical carrier and self-CO-OFDM signal were aligned with a polarization controller in the self-CO-OFDM signal path before detection. Finally, the sampling speed of the digital storage oscilloscope was 80 GS/s, in which the offline receiver DSP was executed in Matlab.

For the case of conventional CO-OFDM, identical parameters as the self-CO-OFDM were adopted, with the exceptions of employing DSP-based frequency-offset compensation with the assistance of pilot subcarriers and not setting any data subcarriers to zero (thus generating 128 subcarriers). In conventional CO-OFDM, the optical carrier was suppressed (−22 dB of OCSR). Moreover, an external cavity laser with 100 kHz linewidth was used as the LO, while the launched optical power of the CO-OFDM was also set at 0 dBm. Three percent (optimum) of the signal band was sacrificed for channel estimation (pilot-aided) in CO-OFDM for both QPSK and 16-QAM. However, in contrast to
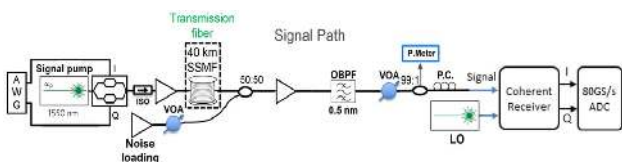
self-CO-OFDM, the nominal S_k dropped to 49.261 and 107.22 Gbit · s^{-1} for QPSK and 16-QAM, respectively; this occurred due to the sacrifice of 5% (QPSK) and 8% (16-QAM) of generated subcarriers for pilot-assisted frequency-offset compensation corresponding to 6 and 10 pilot subcarriers (optimum), respectively.

B. Waveguide Fabrication

Chalcogenide (As$_2$S$_3$) thin films were deposited via thermal evaporation on ⟨100⟩ oriented 100 mm thermal oxide silicon wafers, and a total film thickness of 930 nm was achieved. A ~100 nm layer of SU8 was coated on the wafer before annealing at 130°C for 24 h. Through projection lithography, waveguides with nominal widths of 2.2, 2.4, and 2.6 μm were patterned on the As$_2$S$_3$ layer. The waveguides were designed in spiral coils with waveguide length of 23.7 cm in a physical length of 2 cm. After inductively coupling plasma (ICP), etching an etch depth of 330 nm was targeted and an additional layer of SiO$_2$ was overclad for enhanced acoustic confinement.

C. Simulation Setup and Parameters

The simulation parameters for the developed self-CO-OFDM system, including the 40 km optical link, were identical to the experimental setup, being implemented in a Matlab/Virtual Photonics Inc. (VPI)-transmission-maker co-simulated environment (electrical domain in Matlab and optical components with SSMF in VPI). The SBS noise was modeled as additive-white Gaussian noise (AWGN). The self-CO-OFDM modeling was based on the selective amplification of the carrier with a Lorentzian gain profile (using the optimum SBS gain value) followed by AWGN, whose spectral density was determined from the measured noise figure of the Brillouin amplification process. For the in-line optical amplification, an EDFA was adopted with 8 dB gain and 5.5 dB of noise figure (NF). The EDFA noise was also modeled as AWGN. The SSMF for single-polarization transmission was modeled using the pseudo-spectral split-step Fourier method, which solves the nonlinear Schrödinger equation [2]. The adopted SSMF parameters in this work are the following: fiber nonlinear Kerr parameter, chromatic dispersion, chromatic dispersion-slope, fiber loss, and polarization-mode dispersion coefficient of 1.1 W^{-1} km^{-1}, 16 psnm^{-1} km^{-1}, 0.06 pskm^{-1} (nm^2)$^{-1}$, 0.2 dBkm^{-1}, and 0.1 ps (km$^{0.5}$)$^{-1}$, respectively. Pilot-aided phase-noise compensation was implemented for conventional CO-OFDM, which sacrifices useful signal bandwidth. This is derived from the signal capacity R_{signal} expressions [32] for coherent signals,

$$T_S = \frac{2M_S(1+p)}{r_s}, \tag{1}$$

$$R_{signal} = \sum_{k=1}^{M_S} S_k = \frac{\sum_{k=1}^{M_S} n_k}{T_S} = \frac{r_s \sum_{k=1}^{M_S} n_k}{M_S(1+p)}, \tag{2}$$

where S_k is the signal bitrate corresponding to the kth subcarrier, M_s is the number of subcarriers, n_k is the total number of binary bits conveyed by the kth OFDM subcarrier within one symbol period T_s, r_s is the sampling rate, and p includes the cyclic prefix length to increase the inter-symbol interference tolerance and the total pilot-tune period (related to the pilot-aided symbols for frequency-offset estimation).

4. RESULTS

A. Comparison to a State-of-the-Art Coherent Optical System

In Fig. 5(a), the performance benefit by the on-chip SBS-based self-CO-OFDM is illustrated using QPSK modulation for simplicity. The OSNR was set at 27 dB to isolate the transmitted fiber-induced effects at 40 km from random optical amplification noise (amplified spontaneous emission). In this illustration, digital-based carrier recovery has been neglected for both self-CO-OFDM and CO-OFDM. It is clearly indicated that the received symbols in the QPSK constellation diagram of CO-OFDM are highly distorted, causing phase rotation in contrast to our chip-based approach. This example shows the necessary requirement of state-of-the-art coherent systems for extra DSP-based phase-noise and frequency-offset compensation. In Fig. 5(b), the performance of conventional 16-QAM CO-OFDM is compared to a chip-based 16-QAM self-CO-OFDM at 40 km of transmission using an SBS gain and launched optical power of 14 dB and 0 dBm, respectively. This gain enables performance above the forward-error-correction (FEC)-limit according to a targeted BER [33] of 3.3 × 10^{-3}. For self-CO-OFDM, no phase or frequency-offset correction was applied at the receiver-side DSP; therefore, we investigated a truly self-coherent system. The OCSR, measured as the ratio of the carrier to the level of the signal power from the optical spectrum analyzer (spectral power density), was set at an optimum of ∼ −3 dB in self-CO-OFDM and at −22 dB (suppressed carrier) in CO-OFDM. It should be noted for the case of fiber-based self-CO-OFDM that when the OCSR is very large, the SNRs on neighbor subcarriers of the carrier are reduced compared to the chip because the increased fiber length results in susceptibility to environmental variations, thereby causing performance
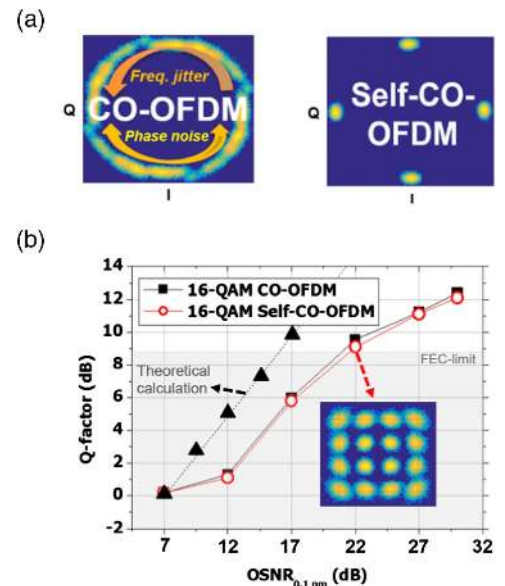
Fig. 5. (a) Comparison of received quaternary phase-shift keying (QPSK) constellation diagrams. (b) Comparison at 40 km: quality (Q)-factor versus optical signal-to-noise ratio (OSNR) for experimental 16-quadrature amplitude modulation (16-QAM). Black triangles refer to the theoretical calculation. The SBS gain and optical carrier-to-signal ratio (OCSR) for the self-coherent system were fixed at 14 dB and −3 dB, respectively. The launched optical power for both systems was fixed at 0 dBm. FEC, forward-error-correction.

penalties, i.e., an increase of both amplitude and phase noise. When the OCSR is too low, the carrier cannot be effectively recovered, since the receiver blurs the carrier with the neighbor subcarriers and also optical amplification noise limits the effectiveness of phase-noise compensation. The results depicted in Fig. 5(b) indicate there is negligible OSNR penalty when including an enhanced carrier. This specifies that the system performance of our method is completely comparable with an optimized coherent optical system, revealing that the recovered carrier with the SBS pump operates similarly to an external cavity laser for practical levels of signal noise. On the other hand, 16-QAM self-CO-OFDM outperforms conventional CO-OFDM in terms of signal capacity by 9.6 Gbit $\cdot$ s^{-1} since pilot-assisted frequency compensation is not necessary.

Compared to the 16-QAM theoretical curve [34], our required OSNR shows an implementation penalty of ~4.7 dB at the FEC limit. We attribute this implementation penalty to bandwidth limitations of the RF components and the modulator; the fact that we did not pre-equalize the drive signals and the additional noise from the coherent receiver, arbitrary waveform generator, and digital storage oscilloscope. Moreover, since pilot-subcarrier-aided phase-noise compensation [35] is implemented in CO-OFDM, sacrificing 8% of the signal, the data rate S_k of 16-QAM self-CO-OFDM is enhanced by 9.6 Gbit $\cdot$ s^{-1} following Eqs. (1) and (2). Pilot-aided algorithms in CO-OFDM can virtually compensate for any residual phase noise from carrier drifting (measured up to 1 MHz). On the contrary, implementing fully blind phase-noise estimation in CO-OFDM is very challenging without considering complex differential bit encoding due to CO-OFDM's long symbol duration and large carrier offset [36]. Finally, it is worth noting that a similar transmission performance is also anticipated from benchmark single-carrier modulation schemes such as Nyquist wavelength division multiplexing [37].

B. Comparison to a Fiber-Based SBS-Self-Coherent OFDM

The chip-based carrier recovery is compared to a fiber-based approach to SBS processing using 4.46 km of SSMF, highlighting the significant drifting in the laser frequency and phase. The reason for using this SSMF was to ensure a single SBS peak, which is critical for this experiment. A fiber with multiple SBS peaks would amplify signals out of band and would also increase the required SBS pump power. The length of the fiber was chosen to (a) achieve high gains with low pump powers while also limiting the added SBS noise and (b) be consistent with other works reported on SBS-based processing [28]. For this demonstration, the impact of the SBS gain and OSNR on the 16-QAM self-CO-OFDM performance is investigated in Fig. 6. The OCSR was maintained at the optimum value of −3 dB. It should be noted that the fiber-based Brillouin gain is also in the saturation regime, similarly to Ref. [28]. In Fig. 6(a), the OSNR was set at a high value of 38 dB to ensure that amplified spontaneous emission noise will not affect our system, keeping the Q-factor within the FEC limit. For low SBS gain, there is no clear distinction between the on-chip and fiber-based SBS. However, for a high gain (>6 dB) on-chip SBS outperforms the fiber-based SBS by up to ~1.2 dB in Q-factor, while at the FEC limit it reduces the maximum required SBS gain by ~2 dB. In Fig. 6(b) the SBS gain was fixed at 14 dB to ensure signal quality well above the FEC limit, validating perfect carrier recovery on the OSNR
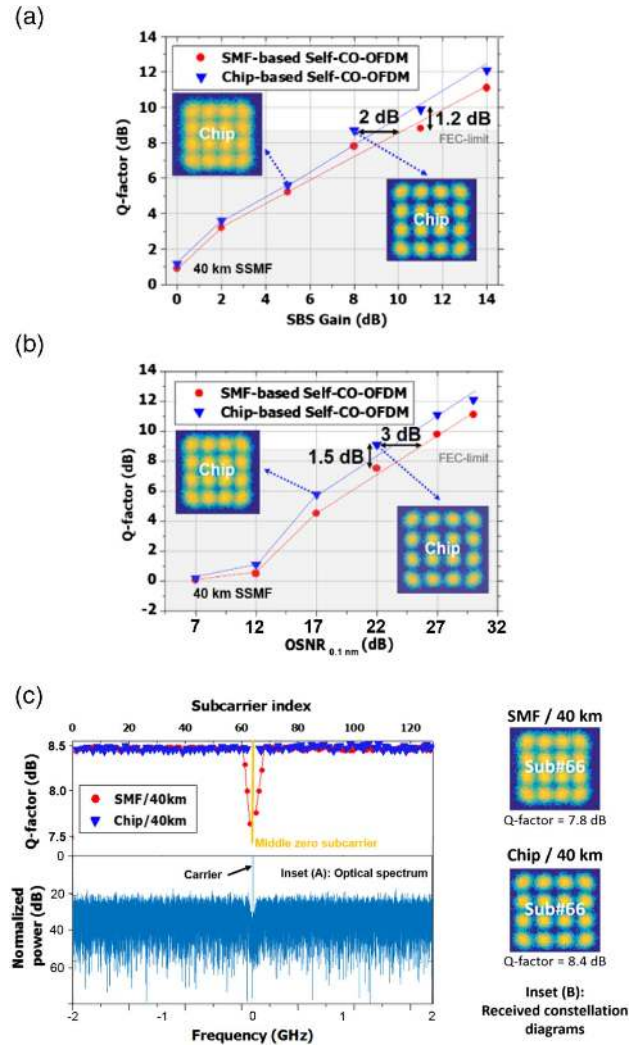
Fig. 6. Comparison of on-chip and fiber-based SBS for 16-QAM self-CO-OFDM. (a) Q-factor versus SBS gain with fixed OSNR at 38 dB and optimum OCSR at −3 dB. (b) Q-factor versus OSNR for best SBS-gain at 14 dB. (c) Subcarrier index (127 subcarriers) versus Q-factor for on-chip and single-mode fiber (SMF)-based SBS with OSNR and gain fixed at 38 and 8 dB, respectively. Inset (A): received optical spectrum with a resolution of 5 MHz after 40 km of SMF transmission. Inset (B): example of received constellation diagrams and Q-factors for subcarrier #66.

evolution. Likewise, for a low OSNR, nearly identical performance is noticeable between chip- and fiber-based SBS. Although, for high OSNR, the on-chip SBS outperforms the fiber-based SBS by up to 1.5 dB in Q-factor and at the FEC limit it extends the required OSNR by 3 dB.

In conclusion, the results here reveal that SBS on a chip outperforms a fiber-based process at high gains. This reveals, for the first time to our knowledge, the technological advantage of using photonic chips over optical fibers beyond the well-established arguments of size, weight, power, and cost (SWAP-C). This indicates that the photonic chip is a necessary component for elimination of excessive carrier drifting and phase noise, resulting in the enhancement of a few subcarriers' SNRs, which are located around the carrier guard band. On the other hand, for low SBS gain, both systems present similar performance since they are dominated by Gaussian noise. The chip-based improved

performance is corroborated in Fig. 6(c), where the individual subcarrier Q-factor is plotted for 16-QAM self-CO-OFDM at 8 dB of SBS gain. To that end, we identify that the Q-factors of the center subcarriers are improved when chip-based SBS is applied due to the cancellation of the residual phase noise. This is explained as follows: in a fiber, SBS suffers more drift because it is longer and exposed more to thermal drifts, at least relative to the chip, which is integrated [38]. This results in the SBS detuning to shift the gain in a fiber, thus boosting the power of the nearest neighbor subcarriers of the carrier, producing unwanted signal–signal beating. These subcarriers are located around the frequency carrier guard band of the OFDM signal, as shown in the received optical spectrum (5 MHz resolution) of inset (A) of Fig. 6(c) related to 40 km transmission. An example of the received constellation diagrams and Q-factors is illustrated in inset (B) for subcarrier #66, revealing an improved Q-factor of 0.6 dB using on-chip SBS.

C. Chip-Based Brillouin Noise Simulation Analysis and Envisioned Chip Solution

In Fig. 7, the impact of SBS noise on the performance of 16-QAM SCO-OFDM is simulated at 40 km transmission and compared with experimental traces. The simulated results are related to an ideally modeled self-CO-OFDM in which frequency drifting was excluded and the OCSR and gain were set similarly to our experiment at –3 dB and 14 dB, respectively. The results are therefore related to chip-based SBS, which has shown no sign of carrier drifting. More details of the modeled self-CO-OFDM are provided in the Methods section. As depicted in Fig. 7, the emulated SBS NF is estimated roughly at maximum 5 dB, considering that there is some implementation penalty. Such levels of NF can be expected for the strong saturation regime of SBS [39–41]. Yet, in comparison to the case of excluding SBS noise, only ~0.95 dB of Q-factor degradation is observed at 30 dB of OSNR (FEC limit). Hence, the simulation analysis shows that the additional noise added to the carrier is equivalent to that added by a 5 dB NF amplifier, indicating that the SBS amplification has a NF comparable with other optical amplification schemes. However, it should be noted that this is a topic of research that warrants further investigation.
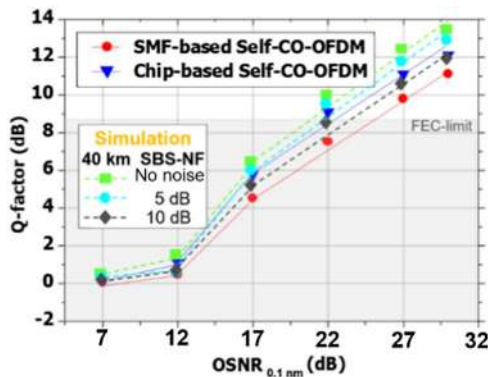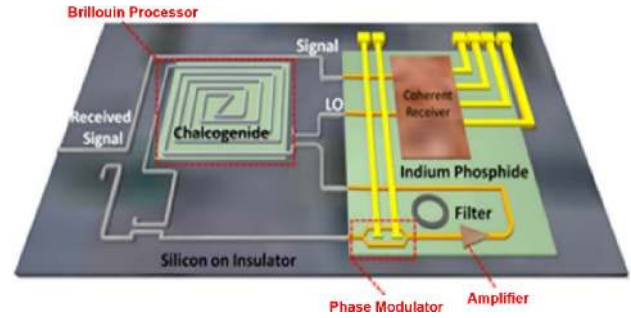
Fig. 8. Envisioned chip-based solution: an integrated photonic chip with carrier recovery and self-coherent detection. In this chip, the chalcogenide (As_2S_3) waveguide [24,25] is used as the phononic processor for providing narrowband Brillouin gain, silicon components to support functional circuits, and indium phosphide for active devices including detectors.

Finally, we propose that full integration of an SBS-self-coherent receiver on a compact photonic chip can potentially further reduce power consumption as well as footprint and weight [41]. Recent progress in developing photonic-chip-based SBS devices offers the potential for integrating optical waveguides that exhibit high SBS gain that, together with critical components such as optical modulators and photodetectors, in a single photonic chip will enhance system stability. An illustration of such envisioned integrated carrier recovery chip combining the Brillouin processor in chalcogenide, the circuits in silicon, and the modulator, filter, amplifier, and coherent receiver in indium phosphide is shown in Fig. 8. To this end, a first step in hybrid integration of silicon and chalcogenide has been taken, where 18.5 dB net Brillouin gain was achieved in a chalcogenide footprint [42] of only 100 μm × 4 mm. In our experiments, a total pump power of ~23 dBm was used to achieve 14 dB of SBS gain. The on-chip power was 19 dBm due to the ~4 dB/facet coupling losses. With optimization of the waveguide design, the propagation losses can be reduced even further, decreasing the required pump power to ~17 dBm, power levels that are compatible with on-chip amplifiers, as shown in Fig. 8. In the current embodiment, external optical amplifiers are required for boosting the pump powers.

5. CONCLUSION

In this work, we reported a novel carrier recovery technique for high-capacity self-coherent optical signals harnessing on-chip SBS that functions as a self-tracking filter. Our demonstration developed a stable and robust all-optical hybrid amplifier-and-filter device that enables record-breaking narrow band of ~265 MHz-bandwidth (a ~485 MHz smaller carrier guard band than Ref. [16] for 16-QAM subcarriers), carrier extraction, and regeneration in self-CO-OFDM without requiring either analog loops or a separate LO laser. The proposed low-complexity system was tested in cost-and-energy-sensitive short-reach telecommunications for signal capacities of up to >100 Gbit·s^{-1} using high-order modulation formats. However, since it has been shown in some previous self-coherent demonstrations [14,43] that nonlinear distortions can be tolerated, it is anticipated that our approach will be considered for longer distances. In contrast to a fiber-based SBS-self-coherent system, our approach provided both phase and polarization stability by neutralizing residual carrier frequency

Fig. 7. SBS noise limit by simulation analysis. Q-factor versus OSNR for 16-QAM self-CO-OFDM with optimum OCSR at –3 dB and best SBS gain at 14 dB (according to Fig. 4). Simulated results for ideal self-CO-OFDM (i.e., no frequency drifting) for different SBS noise figure (NF) are related to 40 km transmission at a launched optical power of 0 dBm.

drifting, without requiring sophisticated carrier-tracking analog devices at the receiver. In comparison to state-of-the-art coherent optical systems, SBS-self-coherent technology discarded the need for digital-based phase noise and frequency-offset compensation, thus relaxing the receiver complexity by removing a DSP functional block without sacrificing transmission performance. To this end, pilot-subcarrier-aided phase-noise compensation was not required for self-coherent OFDM, which wastes useful bandwidth. Moreover, as modulation complexity increases, the computational cost of phase estimation in particular may be increased significantly. Hence, since our approach is fundamentally modulation format independent, it may afford a route to power savings in future systems. In comparison to Stokes receivers [44], our system eliminates the need for two extra photodetectors and relaxes the DSP complexity. On the other hand, as future-proof coherent systems will trigger modulation formats of higher order than 16 states (e.g., 32-QAM–128-QAM), requiring more complex DSP and sophisticated narrower linewidth LOs (<100 kHz) compared to common distributed feedback lasers (>1 MHz), our technique may relax requirements on very-high-order QAM signaling. Our technique is also transparent to higher-spectral-efficient modulation formats (fast-OFDM) [45] and non-orthogonal signal modulation techniques [46]. It should be noted that while the required SBS gain of benchmark fiber-based SBS-self-coherent systems is limited by the modulation format order, being less attractive for higher-order QAM signals compared to homodyne schemes, here, the large SBS gain (52 dB) provided by a chalcogenide chip [24] could potentially support up to 64-QAM [1] and above. Since QAM formats are extremely sensitive to phase and intensity noise [25,47], our experiments confirmed the modest noise added by the narrowband SBS amplifier in a highly saturated regime. It has been shown that noise figure reduces significantly to values comparable to that of an EDFA under strong saturation [39]. The Brillouin amplifier with such a low NF operating over a ~30 MHz bandwidth was the key to increasing the carrier power with respect to the carrier noise without introducing significant noise, therefore enabling successful modulation and demodulation of phase-sensitive signals.

We also believe that the realization of multiple functional devices in a compact photonic chip such as optical modulators and photodetectors could also enhance energy efficiency and system stability—for example, thermal stabilization is easier to achieve for devices integrated on a single chip. On the other hand, the pump power for the SBS gain is close to 20 dBm, which is comparable to the optical power used for LOs in standard coherent receivers. As such, the pump amplifier in our setup should not consume much more power than a LO laser. On-chip filtering can be low loss and so avoid inducing a high-power overhead. While the discrete modulators we use require significant power, on-chip modulators can be made to be very low power (e.g., using capacitive technology [48]). The predominant assumption for photonic integration is that this can reduce the cost of relatively complex optical sub-systems through mass-production of the sub-system itself.

Chip-based SBS-self-coherent optical transport systems are expected to find a wide range of applications to meet the ever-increasing demand of capacity upgrade and cost reduction in future optical networks. However, the proposed hybrid amplifier-filter device can potentially be employed for carrier recovery in other applications—picking out a narrow, "pure" optical tone with high-fidelity, or it could

be useful in precision optical timing over very-long-baseline interferometry (VLBI), which may disclose important findings in fundamental physics and in the search for dark matter [49]. In VLBI, the correlation of signals from distant antennas starts with downconversion and sampling at each telescope that is obtained using a LO whose frequency is referenced to an atomic clock [49]. The spectral purity of the clock is of paramount importance, as in multiplication chains the phase noise is significantly increased, and hence, the atomic clock must exhibit an excellent long-term stability; a loss in the coherence between clocks used in different antennas results in fading of the interferometer fringes. Moreover, our proposed SBS-based device could be used for phase reference sharing in continuous-variable quantum key distribution [50]. Relying on a self-coherent approach, where in this case the phase reference information and quantum information are coherently obtained from a single optical wavefront, very high phase noise can be tolerated [50].

See Supplement 1 for supporting content.

†These authors contributed equally to this work.

REFERENCES

1. M. Pelusi, A. Choudhary, T. A. Inoue, D. Marpaung, B. J. Eggleton, H. N. Tan, K. S. Trapala, and S. Namiki, "Low noise, regeneration of optical frequency comb-lines for 64QAM enabled by SBS gain," in *OptoElectronics and Communications Conference Postdeadline paper* (IEEE, 2016).
2. E. Temprana, E. Myslivets, B. P.-P. Kuo, L. Liu, V. Ataie, N. Alic, and S. Radic, "Overcoming Kerr-induced capacity limit in optical fiber transmission," Science **348**, 1445–1448 (2015).
3. X. Liu, A. R. Chraplyvy, P. J. Winzer, R. W. Tkach, and S. Chandrasekhar, "Phase-conjugated twin waves for communication beyond the Kerr nonlinearity limit," Nat. Photonics **7**, 560–568 (2013).
4. S. T. Le, V. Aref, and H. Buelow, "Nonlinear signal multiplexing for communication beyond the Kerr nonlinearity limit," Nat. Photonics **11**, 570–576 (2017).
5. J. Theodoras, "Ultra low-latency financial networking," ADVA Optical Networking Inc. White paper, 2015, https://www.advaoptical.com/en/resources.
6. K. Bilal, M. Manzano, S. U. Khan, E. Calle, K. Li, and A. Y. Zomaya, "On the characterization of the structural robustness of data center networks," IEEE Trans. Cloud Comput. **1**, 64 (2013).
7. D. T. Van Veen and V. E. Houtsma, "Proposals for cost-effectively upgrading passive optical networks to a 25G line rate," J. Lightwave Technol. **35**, 1180–1187 (2017).
8. B. Bangerter, S. Talwar, R. Arefi, and K. Stewart, "Networks and devices for the 5G era," IEEE Commun. Mag. **52**(2), 90–96 (2014).
9. "Cisco Visual Networking Index: Forecast and Methodology, 2011–2016," Cisco White Paper, 2017, https://www.cisco.com.
10. Alcatel-Lucent, "1830 PSS brochure," https://www.alcatel-lucent.com.
11. "Ciena 6500 product data sheet," https://www.ciena.com.
12. G. Donati, "Optical communications: Kramers-Kronig receiver," Nat. Photonics **10**, 751 (2016).
13. A. Mecozzi, C. Antonelli, and M. Shtaif, "Kramers-Kronig coherent receiver," Optica **3**, 1220–1227 (2016).

14. P. Johannisson, M. Sjodin, M. Karlsson, E. Tipsuwannakul, and P. Andrekson, "Cancellation of nonlinear phase distortion in self-homodyne coherent systems," IEEE Photon. Technol. Lett. **22**, 802–804 (2010).

15. S. Adhikari, S. Sygletos, A. D. Ellis, B. Inan, S. L. Jansen, and W. Rosenkranz, "Enhanced self-coherent OFDM by the use of injection locked laser," in *Optical Fiber Communication Conference* (OSA, 2012), paper JW2A.

16. Z. Liu, J.-Y. Kim, D. S. Wu, D. J. Richardson, and R. Slavík, "Homodyne OFDM with optical injection locking for carrier recovery," J. Lightwave Technol. **33**, 34–41 (2015).

17. T. Miyazaki and F. Kubota, "PSK self-homodyne detection using a pilot carrier for multibit/symbol transmission with inverse-RZ signal," IEEE Photon. Technol. Lett. **17**, 1334–1336 (2005).

18. M. Nakamura, Y. Kamio, and T. Miyazaki, "Linewidth-tolerant real-time 40-Gbit/s 16-QAM self-homodyne detection using a pilot carrier and ISI suppression based on electronic digital processing," Opt. Lett. **35**, 13–15 (2010).

19. M. Sjodin, E. Agrell, P. Johannisson, G.-W. Lu, P. A. Andrekson, and M. Karlsson, "Filter optimization for self-homodyne coherent WDM systems using interleaved polarization division multiplexing," J. Lightwave Technol. **29**, 1219–1226 (2008).

20. L. Xu, J. Hu, D. Qian, and T. Wang, "Coherent optical OFDM systems using self optical carrier extraction," in *Optical Fiber Communication Conference* (OSA, 2008), paper OMU4.

21. S. Adhikari, S. L. Jansen, M. S. Alfiad, B. Inan, A. Lobato, V. A. J. M. Sleiffer, and W. Rosenkranz, "Experimental investigation of self coherent optical OFDM systems using Fabry-Perot filters for carrier extraction," in *European Conference on Optical Communication* (IEEE, 2010), paper Tu.4.A.1.

22. T. Pfau, S. Hoffmann, and R. Noé, "Hardware-efficient coherent digital receiver concept with feedforward carrier recovery for M-QAM constellations," J. Lightwave Technol. **27**, 989–999 (2009).

23. T. Omiya, M. Yoshida, and M. Nakazawa, "400 Gbit/s 256 QAM-OFDM transmission over 720 km with a 14 bit/s/Hz spectral efficiency by using high-resolution FDE," Opt. Express **21**, 2632–2641 (2013).

24. A. Choudhary, I. Aryanfar, S. Shahnia, B. Morrison, K. Vu, S. Madden, B. L. Davies, D. Marpaung, and B. J. Eggleton, "Tailoring of the Brillouin gain for on-chip widely tunable and broadband microwave photonic filters," Opt. Lett. **41**, 436–439 (2016).

25. A. Choudhary, B. Morrison, I. Aryanfar, S. Shahnia, M. Pagani, Y. Liu, K. Vu, S. Madden, D. Marpaung, and B. J. Eggleton, "Advanced integrated microwave signal processing with giant on-chip Brillouin gain," J. Lightwave Technol. **35**, 846–854 (2017).

26. M. Pelusi, A. Choudhary, T. Inoue, D. Marpaung, B. J. Eggleton, K. S. Trapala, H. N. Tan, and S. Namiki, "Frequency comb noise suppressor by a Brillouin comb amplifier for phase sensitive communications," Opt. Express **25**, 17847–17863 (2017).

27. L. Banchi, M. Presi, R. Proietti, and E. Ciaramella, "System feasibility of using stimulated Brillouin scattering in self coherent detection schemes," Opt. Express **18**, 12702–12707 (2010).

28. E. Giacoumidis, E. Magi, A. Choudhary, D. Marpaung, B. Corcoran, M. Pelusi, and B. J. Eggleton, "Enhanced self-coherent optical OFDM using stimulated Brillouin scattering," in *Optical Fiber Communication Conference* (OSA, 2017), paper Th4I.2.

29. R. Haas and J. C. A. Belfiore, "Time-frequency well-localized pulse for multiple carrier transmission," Wireless Personal Commun. **5**, 1–18 (1997).

30. M. S. Erkılınç, D. Lavery, K. Shi, B. C. Thomsen, R. I. Killey, S. J. Savory, and P. Bayvel, "Bidirectional wavelength-division multiplexing transmission over installed fibre using a simplified optical coherent access transceiver," Nat. Commun. **8**, 1043 (2017).

31. A. Choudhary, Y. Liu, B. Morrison, K. Vu, D.-Y. Choi, P. Ma, S. Madden, D. Marpaung, and B. J. Eggleton, "High-resolution, on-chip RF photonic signal processor using Brillouin gain shaping and RF interference," Sci. Rep. **7**, 5932 (2017).

32. E. Giacoumidis, J. L. Wei, X. L. Yang, A. Tsokanos, and J. M. Tang, "Adaptive modulation-enabled WDM impairment reduction in multichannel optical OFDM transmission systems for next generation PONs," IEEE Photon. J. **2**, 130–140 (2010).

33. R. C. Bose and D. K. Ray-Chaudhuri, "On a class of error correcting binary group codes," Inf. Control **3**, 68–79 (1960).

34. R.-J. Essiambre, G. Kramer, P. J. Winzer, G. J. Foschini, and B. Goebel, "Capacity limits of optical fiber networks," J. Lightwave Technol. **28**, 662–701 (2010).

35. E. Giacoumidis, M. A. Jarajreh, S. Sygletos, S. T. Le, A. Tsokanos, A. Hamié, E. Pincemin, Y. Jaouën, F. Farjady, A. D. Ellis, and N. J. Doran, "Dual-polarization multi-band OFDM transmission and transceiver limitations for up to 500 Gb/s in uncompensated long-haul links," Opt. Express **22**, 10975–10986 (2014).

36. S. T. Le, P. A. Haigh, A. D. Ellis, and S. K. Turitsyn, "Blind phase noise estimation for CO-OFDM transmissions," J. Lightwave Technol. **34**, 745–753 (2016).

37. M. A. Soto, M. Alem, M. A. Shoaie, A. Vedadi, C.-S. Brès, L. Thévenaz, and T. Schneider, "Optical sinc-shaped Nyquist pulses of exceptional quality," Nat. Commun. **4**, 2898 (2013).

38. A. Zarifi, B. Stiller, M. Merklein, N. Li, K. Vu, D.-Y. Choi, P. Ma, S. J. Madden, and B. J. Eggleton, "Highly localized distributed Brillouin scattering response in a photonic integrated circuit editors-pick," APL Photon. **3**, 036101 (2018).

39. A. Choudhary, M. Pelusi, D. Marpaung, T. Inoue, K. Vu, P. Ma, D.-Y. Choi, S. Madden, S. Namiki, and B. J. Eggleton, "On-chip Brillouin purification for frequency comb-based coherent optical communications," Opt. Lett. **42**, 5074–5077 (2017).

40. Y. Souidi, F. Taleb, J. Zheng, M. W. Lee, F. D. Burck, and V. Roncin, "Low-noise and high-gain Brillouin optical amplifier for narrowband active optical filtering based on a pump-to-signal optoelectronic tracking," Appl. Opt. **55**, 248–253 (2016).

41. J. Pfeifle, V. Brasch, M. Lauermann, Y. Yu, D. Wegner, T. Herr, K. Hartinger, P. Schindler, J. Li, D. Hillerkuss, R. Schmogrow, C. Weimann, R. Holzwarth, W. Freude, J. Leuthold, T. J. Kippenberg, and C. Koos, "Coherent terabit communications with microresonator Kerr frequency combs," Nat. Photonics **8**, 375–380 (2014).

42. B. Morrison, A. C. Bedoya, G. Ren, K. Vu, Y. Liu, A. Zarifi, T. G. Nguyen, D.-Y. Choi, D. Marpaung, S. J. Madden, A. Mitchell, and B. J. Eggleton, "Compact Brillouin devices through hybrid integration on silicon," Optica **4**, 847–854 (2017).

43. J. Jignesh, A. Lowery, and B. Corcoran, "Inter-channel nonlinear phase noise compensation using optical injection locking," Opt. Express **26**, 5733–5746 (2018).

44. P. Dong, X. Chen, K. Kim, S. Chandrasekhar, Y.-K. Chen, and J. H. Sinsky, "128-Gb/s 100-km transmission with direct detection using silicon photonic Stokes vector receiver and I/Q modulator," Opt. Express **24**, 14208–14214 (2016).

45. E. Giacoumidis, A. Tsokanos, C. Mouchos, G. Zardas, C. Alves, J. L. Wei, J. M. Tang, C. Gosset, Y. Jaouën, and I. Tomkos, "Extensive comparisons of optical fast-OFDM and conventional optical OFDM for local and access networks," J. Opt. Commun. Netw. **4**, 724–733 (2012).

46. J. Zhou, Y. Qiao, Z. Yang, Q. Cheng, Q. Wang, M. Guo, and X. Tang, "Capacity limit for faster-than-Nyquist non-orthogonal frequency-division multiplexing signaling," Sci. Rep. **7**, 3380 (2017).

47. K. Kikuchi, "Fundamentals of coherent optical fiber communications," J. Lightwave Technol. **34**, 157–179 (2016).

48. C. Milivojevic, C. Raabe, A. Shastri, M. Webster, P. Metz, S. Sunder, B. Chattin, S. Wiese, B. Dama, and K. Shastri, "112 Gb/s DP-QPSK transmission over 2427 km SSMF using small-size silicon photonic IQ modulator and low-power CMOS driver," in *Optical Fiber Communication Conference/National Fiber Optic Engineers Conference*, OSA Technical Digest (Optical Society of America, 2013), paper OTh1D.1.

49. C. Clivati, R. Ambrosini, T. Artz, A. Bertarini, C. Bortolotti, M. Frittelli, F. Levi, A. Mura, G. Maccaferri, M. Nanni, M. Negusini, F. Perini, M. Roma, M. Stagni, M. Zucco, and D. Calonico, "A VLBI experiment using a remote atomic clock via a coherent fibre link," Sci. Rep. **7**, 40992 (2017).

50. A. Marie and R. Alléaume, "Self-coherent phase reference sharing for continuous-variable quantum key distribution," Phys. Rev. A **95**, 012316 (2017).